Experimental and theoretical investigation on critical cutting force in rotary ultrasonic drilling of brittle materials and composites

Jianjian Wang [a,b], Jianfu Zhang [a], Pingfa Feng [a,c,*], Ping Guo [b]

[a] Beijing Key Lab of Precision/Ultra-precision Manufacturing Equipment and Controls, Tsinghua University, Beijing, China
[b] Department of Mechanical and Automation Engineering, The Chinese University of Hong Kong, Hong Kong, China
[c] Division of Advanced Manufacturing, Graduate School at Shenzhen, Tsinghua University, Shenzhen, China

ARTICLE INFO

ABSTRACT

Rotary ultrasonic drilling (RUD) has been fully proved to be superior in hole-manufacturing of brittle materials and composites with reduced cutting force and improved machining quality. This paper was devoted to the proposition of a novel index for the design and manufacturing of an ultrasonic machine tool (RUMT), called the critical cutting force, to characterize the RUMT maximum processing capacity. When the cutting force exceeded this critical value, the ultrasonic amplitude decreased and the cutting force increased abruptly, resulting in the RUD superiority suppression. The critical cutting force dependency was investigated theoretically and experimentally. Firstly, the effect of cutting force on the ultrasonic amplitude stability was modeled and subsequently verified by experimental results on both quartz glass and C/SiC composites. It was indicated that the effect of material properties on the amplitude stability could be attributed to the cutting force variation no matter the material is composite or not. Following, a critical cutting force model was developed mechanistically with consideration to the interactive action between the cutting force and the ultrasonic vibration. The modeling results demonstrated that the critical cutting force was an inherent property of RUMT dependent on the corresponding excitation level and independent of the processing conditions. The experimental results on quartz glass, sapphire and C/SiC composites verified the model predictive ability and the critical cutting force independency of the processing conditions such as feedrate, spindle speed, material properties and even tool wear.

© 2017 Elsevier Ltd. All rights reserved.

1. Introduction

Hard and brittle materials that are represented by optical glass, advanced ceramics and ceramic matrix composites, have a wide range of industrial applications due to the corresponding excellent mechanical and chemical performances. In contrast, due to the corresponding high hardness and low toughness, the hard and brittle materials are regarded as the most difficult-to-machine materials. The rotary ultrasonic machining (RUM) has been sufficiently proved to be a superior machining method, especially of hole-manufacturing for hard and brittle materials with reduced cutting force and subsurface damage, improved hole exit quality and extended tool life [1–3]. In RUM, a diamond core tool vibrates longitudinally in an ultrasonic frequency with amplitudes of micrometers, simultaneously feeding towards the workpiece. A certain RUM machine tool (RUMT) can be used for not only hole drilling but also face milling, namely rotary ultrasonic drilling (RUD, as presented in Fig. 1(a)) and rotary ultrasonic face milling (RUFM). Due to the cor-

responding promising performance and application potential, the RUM has attracted high attention in the fields of difficult-to-cut material processing [1].

A high number of typical and widely utilized difficult-to-cut materials have been successfully machined by RUM, such as the optical glass [4–6], the sapphire [7], the silicon carbide [8], the C/SiC [9,10], the CFRP [11,12], the CFRP/Ti [13], the titanium alloy [14], the KDP crystal [15], the glass ceramics [16], the SiC_p/Al [17] and the zirconia [18]. Besides experimental investigations on the processing performance of RUM, the theoretical modeling of processing outputs was also paid significant attention to by academics and industry engineers. Pei et al. mechanistically developed a model of material removal rate (*MRR*) in RUM of brittle materials based on the indentation fracture mechanics [19]. This model was quite fundamental and far-reaching that nearly all following modeling works were established on it. As an example, several cutting force models have been developed based on the *MRR* model by Liu et al. [20], Cong et al. [21], Yuan et al. [22], Zhang et al.

[23] and Xiao et al. [18], with consideration to the differences in material types and machining types (drilling or milling). Bertsche et al. also developed a radial cutt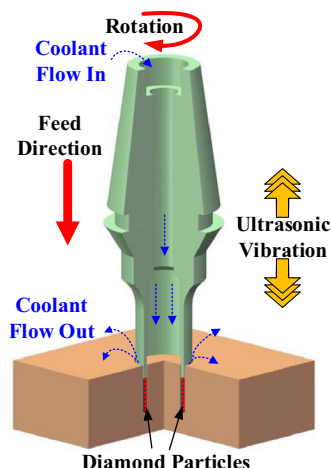ing force model for RUM based on the macro and micro kinematic analysis of tool, diamond grain and workpiece [24]. Feng et al. focused on the modeling work and suppression methods in terms of RUM induced damages, such as edge chipping at the hole exit and subsurface damage [25,26]. Lv et al. also developed a model to predict the subsurface damage in the RUM of an optical glass [27]. These models established the dependency of processing outputs on the inputs and facilitated the improved RUM technology application. Moreover, the other research trends of RUM were the corresponding performance promotion through the complex vibration utilization, such as the elliptical vibration substitution of the conventional longitudinal vibration [12,28,29].

In all aforementioned researches, the stable ultrasonic amplitude was assumed against various processing conditions. Therefore, the processing parameters were always selected indifferently to the interactive effects between ultrasonic parameters (frequency and amplitudes) and grinding parameters (spindle speed, feedrate). In other words, the effect of material removal on the stability of ultrasonic amplitude was generally neglected. In contrast, as a typical ultrasonic assisted machining technology, the RUM is supposed to be sensitive to the tuning frequency of RUMT and the mechanical load, due to material removal. Actually, certain critical aspects have been reported to exist in other ultrasonic assisted machining technologies. As an example, Astashev et al. discovered that when the static driving force ultrasonic machining (USM) exceeded a critical value, the MRR would decrease to zero due to the ultrasonic amplitude suppression [30]. Shamoto et al. reported a critical nominal clearance angle of the cutting tool that guaranteed the always-positive instantaneous clearance angle during elliptical vibration cutting [31]. Brehl et al. calculated a critical upfeed velocity below which, most benefits of vibration assisted cutting would be derived from the periodic separation of the tool rake face from the uncut material. Similarly, especially in RUD, according to the authors' previous study [32], a critical feedrate exists, below which the superior performance of RUD would be effective in terms of significant cutting force reduction. In contrast, the critical feedrate of RUD is dependent on too many factors such as the spindle speed, the tool wall thickness, the abrasive size and the material properties. Moreover, the feasibility of critical feedrate during brittle composites drilling is not involved in the authors' previous study [32], though the ceramic matrix composite was also an important machining object of the RUMT. The potential effect of material removal of brittle composites on the critical aspect of RUD was not clear. It was difficult and troublesome for the critical feedrate model utilization to guide the manufacturing and application of the RUMT directly.

Considering RUD apart from RUFM is one of most important and mature application of RUM technology, this paper was devoted to a novel critical aspect proposition of RUD, called the critical cutting force that was significantly fundamental compared to the critical feedrate. It would be derived theoretically and verified experimentally that the critical cutting force was an inherent property of RUMT, which was independent of the material type and properties, and of the processing parameters, such as the spindle speed, the drilling depth, the tool wear and the feedrate. The critical cutting force was suggested as a novel design index for the RUMT. Moreover, the potential effect of brittle composites and the methods for the critical cutting force improvement of RUMT were also discussed.

2. Mechanistic modeling

The model of critical cutting force in RUD of brittle materials and composites was developed and described step by step in this chapter. Firstly, the cutting force dependency on the processing parameters, especially on the actual ultrasonic amplitude was established. Consequently, the cutting force effect on the stability of ultrasonic vibration was modeled based on the RUMT model, given an idle ultrasonic amplitude. Finally, the critical cutting force model was derived.
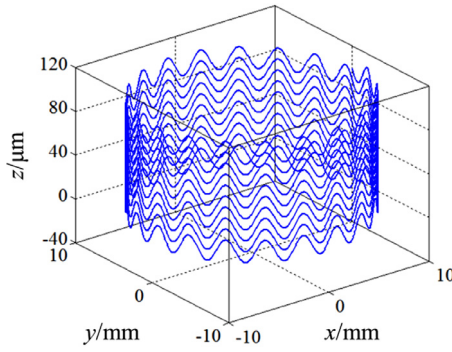

Fig. 1. Illustration of RUD.

Fig. 2. Trajectory of diamond abrasive in RUD.

2.1. Dependency of cutting force on processing parameters

The cutting force model development was derived from the material removal mechanism in the RUD of brittle materials. The abrasives electroplated on the tool end face accomplished the dominant material removal of RUD. As presented in Fig. 1, the movement of diamond abrasive combined the rotational motion, the longitudinal feed motion and the longitudinal ultrasonic vibration. The trajectory movement of the diamond abrasive during RUD can be expressed as:

$$S_{RUM}(t) = \begin{bmatrix} R\cos(\frac{2\pi S}{60}t) \\ R\sin(\frac{2\pi S}{60}t) \\ A\cos(2\pi ft) + f_r t \end{bmatrix} \quad (1)$$

where, t is the processing duration, R is the tool average radius, f is the tuning frequency of RUMT, A is the actual ultrasonic amplitude, S is the spindle speed in rpm and f_r is the longitudinal feedrate. Fig. 2 presents the trajectory of a diamond abrasive obtained from Eq. (1).

In RUD, the diamond abrasives could be considered as multiple Vickers indenters. These indenters impacted the workpiece surface and removed the material in the mode of brittle fracture. Due to the tool ultrasonic vibration, the diamond abrasives were not always in contact with the workpiece material. As presented in Fig. 2, in each vibration cycle, the diamond abrasives on the tool end face penetrated the workpiece material for a certain period of time, called the effective contact duration (Δt), with a maximum depth of δ.

Because the longitudinal feedrate of tool was significantly lower than the vibrational velocity, such as $f_r \ll 2\pi fA$, the $.f_r$. can be neglected during the of contact duration Δt calculation. From Eq. (1), the Δt can be derived as:

$$\Delta t = \frac{1}{\pi f}\arccos(1 - \frac{\delta}{A}) \quad (2)$$

Through the $\arccos(1 - \delta/A) \approx \sqrt{2\delta/A}$ to simplify Eq. (2), the Δt can be calculated as:

$$\Delta t \approx \frac{\sqrt{2}}{\pi f}(\frac{\delta}{A})^{\frac{1}{2}} \quad (3)$$

According to the results of Jiao et al. [33], the maximum impact force of a single diamond abrasive F_n can be expressed as a function of the penetration depth:

$$F_n = \frac{1}{2}\xi\delta^2\tan^2\psi H_V \quad (4)$$

where, ξ is the geometrical factor of the indenter, ψ is semi-vertical angle of the indenter, H_V is the micro hardness of the workpiece material.

With the assumption that all effective abrasives that took part in the material removal, penetrated the workpiece material with the same maximum depth of δ, the maximum impact force F_m of all abrasives can be calculated as:

$$F_m = mF_n \quad (5)$$

where, m is the number of effective abrasives. As presented in Fig. 2, a triple wave could be utilized to simplify the actual cutting force as follows:

$$F(t) = \begin{cases} \frac{F_m}{2\Delta t}t + F_m, & -\Delta t < t < 0 \\ -\frac{F_m}{2\Delta t}t + F_m, & 0 < t < \Delta t \end{cases} \quad (6)$$

Consequently, according to the theorem of impulse, the average cutting force F_c can be derived as:

$$\frac{F_c}{f} = \frac{F_m\Delta t}{2} \quad (7)$$

Through the substitution of Eqs. (3)–(5) into Eq. (7), it could be obtained:

$$F_n = \left[\frac{\pi}{m}\right]^{\frac{4}{5}} \cdot [\tan\psi A]^{\frac{2}{5}} \left[2\xi H_V\right]^{\frac{1}{5}} \cdot F_c^{\frac{4}{5}} \quad (8)$$

As illustrated in Fig. 4(a), the material removal during the RUD of brittle materials was regarded as an indentation fracture process. The lateral and medial cracks were produced during the diamond abrasives penetration. The radial cracks remained beneath the workpiece surface as the subsurface damage. The lateral cracks propagated and interacted with each other, leading to the material removal. The length C_L and depth C_h of the lateral crack can be expressed as [34]:

$$\begin{cases} C_L = C_2(\cot\psi)^{5/12}\left(\frac{E^{3/4}}{H_V K_{IC}(1-v^2)^{1/2}}\right)^{1/2}F_n^{5/8} \\ C_h = C_2(\cot\psi)^{1/3}\frac{E^{1/2}}{H_V}F_n^{1/2} \end{cases} \quad (9)$$

where, E, v and K_{IC} represent the elastic module, the Poisson's ratio and the fracture toughness of the workpiece material, respectively and C_2 is an constant factor, $C_2 = 0.226$ [34].

In Fig. 4(b), $B_0B_1B_2B_3B_4$ is the theoretical material removal volume of a single abrasive, where L_s is the scratching length of a single abrasive on the material surface during one vibration period and it could be derived as:

$$L_s = \frac{\pi RS\Delta t}{30} \quad (10)$$

Consequently, the theoretical material removal volume V_0 of a single abrasive could be calculated as:

$$V_0 = \frac{C_L C_h L_s}{3} \quad (11)$$

Therefore, the material removal rate MRR of all abrasives is:

$$MRR = K_V \cdot V_0 \cdot f \cdot m \quad (12)$$

where, K_v is the actual material removal volume ratio of a single abrasive to the theoretical material removal volume. Simultaneously, the MMR can be calculated from the tool feed motion:

$$MRR = f_r S_0 \quad (13)$$

where, S_0 is the tool end face area. Because the thickness c_0 of the tool wall is relatively significantly lower than the tool radius R, the S_0 can be simplified as:

$$S_0 \approx 2\pi Rc_0 \quad (14)$$

According to Eqs. (10)–(14), it can be obtained:

$$K_V \cdot \frac{C_L C_h}{3} \cdot \frac{\pi RS\Delta t}{30} \cdot f \cdot m = 2\pi Rc_0 f_r \quad (15)$$

Through Eqs. (3), (4), (8) and (9) substitution into Eq. (15), the cutting force F_c can be derived as:

$$F_c = \left[\frac{90 H_V^{59/40} K_{IC}^{1/2}(1-v^2)^{1/4}m^{\frac{1}{10}}c_0 f_r}{\pi^{\frac{1}{10}}\xi^{1/40}K_V C_2^2 E^{7/8}(\tan\psi)^{3/10}A^{\frac{1}{20}}S}\right]^{\frac{10}{11}} \quad (16)$$

Eq. (16) established the relationship among the cutting force F_c and the processing parameters including spindle speed, feedrate, ultrasonic amplitude, tool parameters and material properties in the RUD of brittle

materials. When brittle composites are machined, the material properties E, v, K_{IC} and H_V in Eq. (16) could utilize the equivalent values obtained by the experiments or mixing rule of the composites. Actually, the dependency of cutting force on processing parameters is so significant not only in RUD but also in RUFM [24].

2.2. Effect of cutting force on ultrasonic amplitude stability

According to Astashev et al. [30], a typical machine for power ultrasonic process could be modeled as in Fig. 5. The RUD is a typical power ultrasonic process; consequently the RUMT could also be modeled as in Fig. 5. As presented in Fig. 5, the load on the tool from material removal was represented by $\tilde{F}$, the actual complex ultrasonic amplitude of the tool during machining was represented by $\tilde{a}$.

According to Astashev et al. [30], the relationship between the actual complex ultrasonic amplitude $\tilde{a}$ under load and the idle complex ultrasonic amplitude $\tilde{a}_0$ without load for a general ultrasonic system can be expressed as:

$$\tilde{a} = \tilde{a}_0 \frac{W_M(j \cdot 2\pi f)}{W_M(j \cdot 2\pi f) + W_H(j \cdot 2\pi f)} \tag{17}$$

where, $W_M(j \cdot 2\pi f)$ is the dynamic stiffness of the RUMT which relates the displacement of the tool to the forces acting upon it. $W_H(j \cdot 2\pi f)$ is the dynamic stiffness which relates the ultrasonic amplitude $\tilde{a}$ to the load $\tilde{F}$ of the ultrasonic process and:

$$\tilde{F} = W_H(j \cdot 2\pi f)\tilde{a} \tag{18}$$

$W_M(j \cdot 2\pi f)$ and $W_H(j \cdot 2\pi f)$ can be written as:

$$\begin{cases} W_M(j \cdot 2\pi f) = U_M(2\pi f) + jV_M(2\pi f) \\ W_H(j \cdot 2\pi f) = k(A) + j\omega b(A) \end{cases} \tag{19}$$

where, $A = |\tilde{a}|$, U_M and V_M are the real and imaginary parts of W_M respectively, k and b are the equivalent stiffness and the load damping from the material removal respectively.

Generally, the RUMT was tuned at the corresponding idle resonant frequency f_0 without machining. At this time frame, the U_M and V_M can be calculated as:

$$\begin{cases} U_M(2\pi f_0) = 0 \\ V_M(2\pi f_0) = V_{M0} \end{cases} \tag{20}$$

where, V_{M0} is the energy consumption parameter of RUMT.

By the harmonic linearization method application for Eq. (6), the $k(A)$ and $b(A)$ can be calculated as:

$$\begin{cases} k(A) = \frac{2}{TA} \int_0^T F(t)\cos(2\pi f t)dt \approx \frac{2F_c}{A} \\ b(A) = -\frac{1}{T\pi f A} \int_0^T F(t)\sin(2\pi f t)dt = 0 \end{cases} \tag{21}$$

With Eqs. (19)–(21) substitution into Eq. (17), and by modulus operation, the actual ultrasonic amplitude A during machining process can be derived as:

$$A = \frac{A_0 V_{M0}}{\sqrt{\left(\frac{2F_c}{A}\right)^2 + V_{M0}^2}} \tag{22}$$

where, $A_0 = |\tilde{a}_0|$ is the idle ultrasonic amplitude without machining.

On the other hand, according to the authors' previous study, the ultrasonic power that the RUMT consumes can be expressed as [35]:

$$\begin{cases} P_{A_0} = \pi f_0 V_{M0} A_0^2 + P_0 \\ P_A = \pi f_0 V_{M0} A^2 + P_0 \end{cases} \tag{23}$$

where, P_A and P_{A_0} are the ultrasonic power that RUMT consumes when the ultrasonic amplitude of the tool are A and A_0 respectively, P_0 is the electric power that RUMT consumes when the ultrasonic amplitude is zero.

With Eq. (22) substitution into Eq. (23), the variation of ultrasonic power ΔP due to the effect of cutting force can be derived as:

$$\Delta P = \frac{4\pi f_0}{V_{M0}} F_c^2 \tag{24}$$
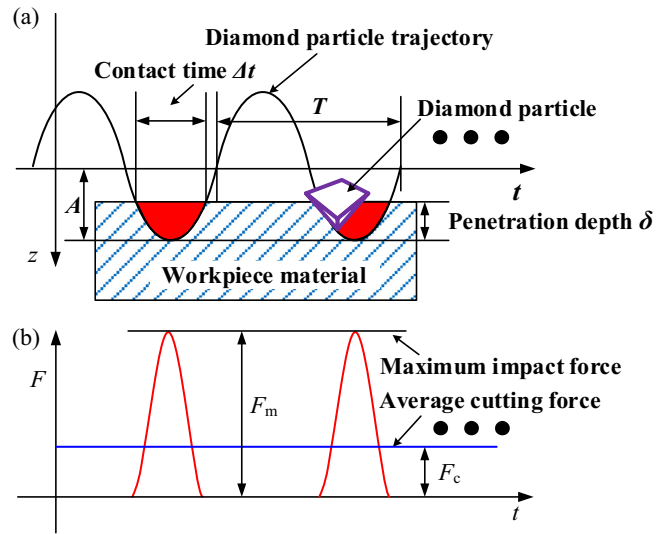
where $\Delta P = P_{A_0} - P_A$.

Fig. 3. (a) Effective contact duration in single ultrasonic vibration cycle, (b) wave profile of cutting force.

2.3. Critical cutting force and its dependency on RUMT's properties

According to Eq. (16), the relationship between the cutting force F_c and the actual ultrasonic amplitude A during machining process can be written as:

$$F_c = \lambda A^{-\chi} \tag{25}$$

where, χ is the constant index, whereas λ is a coefficient that depends on drilling conditions such as feedrate, spindle speed, abrasives, lubrication, chip discharging and material properties.

With Eq. (25) substitution into Eq. (22), it could be obtained:

$$\lambda = \frac{V_{M0}}{2}\sqrt{A_0^2 - A^2}A^{-\chi} \tag{26}$$

Eq. (26) established the relationship among the drilling conditions and the actual ultrasonic amplitude. As well known that, the average cutting force F_c significantly depends on processing parameters. According to Eqs. (25) and (26), if the processing parameters related λ increases (such as feedrate increase [32]), the A decreases, therefore the average cutting force F_c increases. In Eq. (26), according to the knowledge of functions, when $A = A_0\sqrt{\chi/(\chi+1)}$, processing parameters related λ reaches the corresponding extreme value. The physical significance of the extreme value of λ is that, if the λ continues to increase exceeding its extreme value, Eq. (26) would not be balanced ever resulting in the ineffectiveness of RUD. When the λ reaches its extreme value, simultaneously average cutting force F_c reaches the corresponding extreme value, called the critical cutting force $F_{c,critical}$:

$$F_{c,critical} = \frac{V_{M0} A_0}{2\sqrt{1 + \chi}} \tag{27}$$

where, $V_{M0} A_0$ represents the excitation level of RUMT, which could be adjusted during the RUMT design and manufacturing. Eq. (27) indicated that the critical cutting force was an inherent property of RUMT (no dependency on λ) characterizing the RUMT maximum processing capacity, therefore proving suitable as a design and manufacture index of RUMT's.

Due to the tool ultrasonic vibration, the actual cutting force during RUD varied ultrasonically. The critical cutting force of Eq. (27) is the average value of actual cutting force, whereas not the maximum value as illustrated in Fig. 3(b). By the Fourier transformation method application, the actual cutting force could be extracted from a direct current component (namely the average value) and the series of ultrasonic frequency components. According to Eqs. (17)–(19), it is the ultrasonic frequency components of the actual cutting force that affect the stability of
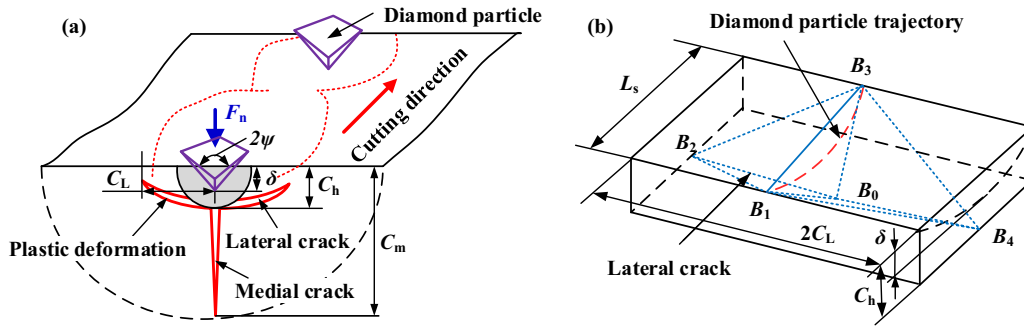
Fig. 4. (a) Crack system of indentation fracture, (b) calculation of material removal volume.
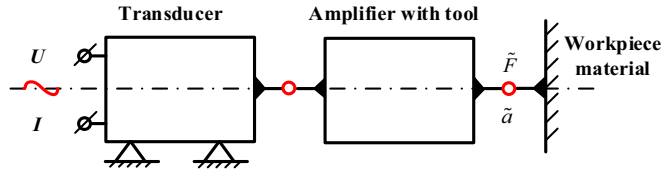

Fig. 5. A model of RUMT.

ultrasonic vibration [30]. In contrast, Eq. (21) developed the relationship among the average value and the ultrasonic frequency components of the cutting force. Therefore, it proved practicable to utilize the average value of actual cutting force to characterize the critical cutting force.

Furthermore, the resonant frequency of the dynamometer was quite low (would become quite lower once it was mounted with the workpiece) compared to the ultrasonic vibration frequency. As an example, the resonant frequency of the precise Kistler 9256C2 dynamometer was only 4.6 kHz. It was impossible to acquire the force variation within a vibration cycle regardless of any high sampling frequency. Though the ultrasonic frequency components of the actual cutting force could not be measured effectively due to the significantly lower resonant frequency of the dynamometer, the direct current component of the actual cutting force could be measured with an appropriate accuracy. Therefore, it was beneficial for the critical cutting force application if the average value of the actual cutting force is utilized, the availability consideration of the cutting force' components.

3. Experimental procedure

3.1. Experimental setup

The experiments were conducted in a RUMT Ultrasonic 50 that was produced by DMG, in Germany. The tuning frequency range of the Ultrasonic 50 was 16.5 kHz–30 kHz. As presented in Fig. 6, the Ultrasonic 50 comprised an ultrasonic spindle system (model HSK63-S), a numerical control machining system and a coolant system. The ultrasonic spindle system was the key component of Ultrasonic 50. It consisted of an ultrasonic spindle and a power supply. The power supply with a maximum output ultrasonic power of 300 W, converted the 50 Hz electrical current into the ultrasonic frequency AC output for the ultrasonic spindle. The ultrasonic spindle, with a maximum rotating speed of the ultrasonic spindle of 6000 rpm in ultrasonic mode, consisted of a piezoelectric transducer, an ultrasonic horn and a diamond core tool. The piezoelectric transducer converted the AC input into ultrasonic mechanical vibrations. The ultrasonic horn amplified the ultrasonic vibrational amplitude into the applicable magnitude mechanical machining. The components of ultrasonic spindle should be well designed to guarantee a considerable vibration amplitude.
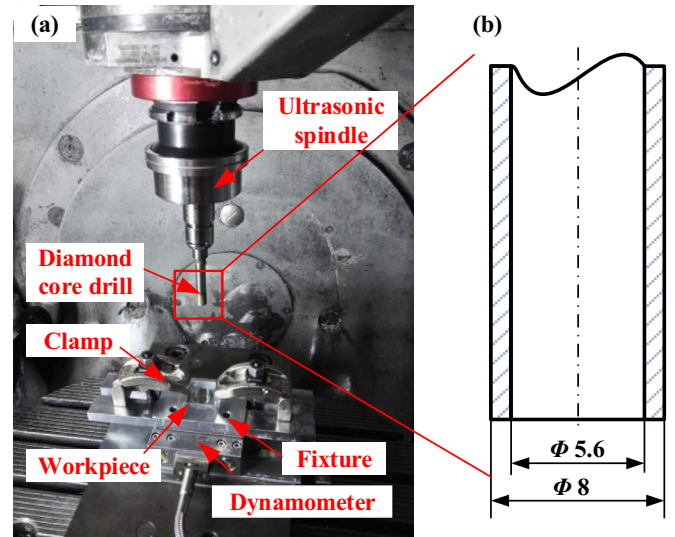

Fig. 6. (a) Experimental setup and (b) dimension of diamond core tool.

As presented in Fig. 6, an electroplated diamond core tool that was closer to a ring with diamond powder was utilized in the experiments. The corresponding grit size was D76, the outside diameter was 8 mm and the wall thickness was 1.2 mm. The diamond core tool was connected to the ultrasonic horn by an ER16 cone fit. Simultaneously, a fixture mounted on a piezoelectric dynamometer (model 9256C2, Kistler Instrument Corp.) was utilized to hold the specimen by two clamps. The ultrasonic power was read from the RUMT operation panel.

The dynamometer was utilized to measure the cutting forces along the longitudinal direction of the tool during the drilling experiments. The cutting electrical signal force from the dynamometer was amplified by an amplifier (5070A) and consequently fed to a data recorder. The recorded cutting force was subsequently saved and processed by commercial software (Dynoware, Kistler Instrument Corp.) Generally, in order to capture the variation of actual cutting force in ultrasonic frequency, the sampling frequency of cutting force measurement should at least double the ultrasonic frequency. However, because the resonant frequency of the dynamometer (Kistler 9256C2) was quite low (4.6 kHz) compared to the ultrasonic vibration frequency. Moreover, the resonant frequency of force measurement system would become quite lower once it was mounted with the workpiece. Therefore, it was impossible to acquire the force variation accurately within a vibration cycle. The increase of sampling frequency was ineffective in this situation. Following, as it has been discussed in Section 2.3, it proved practicable to utilize the direct current component of actual cutting force to characterize the critical cutting force. Furthermore, the direct current component of the actual cutting force, namely the average cutting force, could be measured with an appropriate accuracy at relatively low sampling rate.
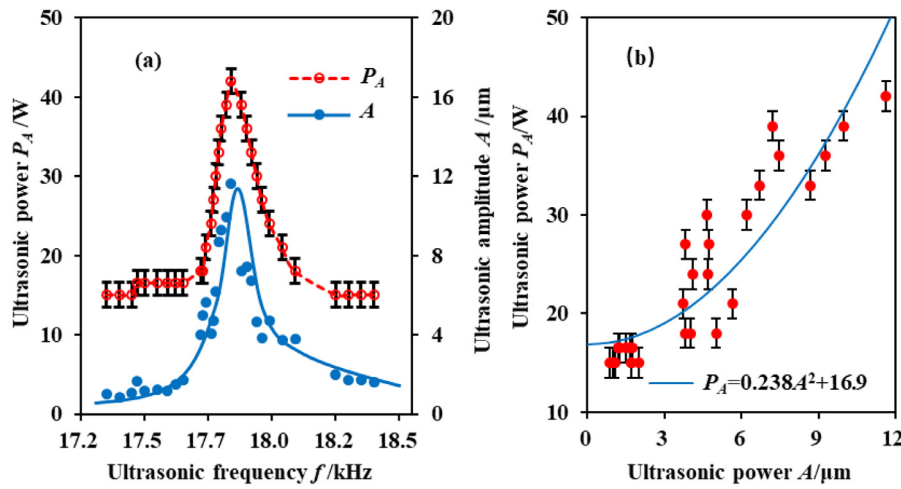
Fig. 7. (a) Dependency of ultrasonic power and amplitudes on frequency, (b) relationship between ultrasonic power and amplitudes [32].

Consequently, the sampling frequency of the cutting force measurement was set at 1000 Hz.

As explained in Section 2.3, the direct current component of the actual cutting force, namely the average cutting force, could be measured with an appropriate accuracy by low-frequency dynamometer. The raw data of measured cutting force contain sufficient information regarding the average cutting force, together with unavoidable noises. In this study, a widely applied data analysis method, namely the simple moving average method (1000 window size equivalent to sampling frequency) was used through Dynaware to obtain the variation tendency of average cutting force with increase of drilling depth. The moving average method is usually applied with time series data to clear away short-term fluctuations and highlight longer-term trends [36].

3.2. Experiments to obtain V_{M0}

In the model of critical cutting force, as expressed by Eq. (27), the V_{M0} is an important parameter which characterized the energy consumption ability of RUMT. As illustrated by Eq. (23), the RUMT with a higher V_{M0} consumes more energy. For a certain RUMT, the V_{M0} could be obtained by the ultrasonic power and amplitudes measurements.

A group of experiments for the ultrasonic power and amplitudes measurements were performed to obtain the amplitude-frequency characteristics of Ultrasonic 50 with the aforementioned tool at idle mode. The frequency values were set from 17.30 kHz to 18.35 kHz to tune the RUMT discontinuously. The ultrasonic amplitude was measured by a laser fiber vibrometer (LKH008, KEYENCE, Japan), which had a maximum sampling frequency of 392 kHz and a resolution ratio of 0.1 μm. The ultrasonic amplitudes were derived from the sine curve obtained by the laser spot focusing at the tool end face when the tool was vibrating. Fig. 7 demonstrates the measuring results, such as the relationship between the ultrasonic power and the amplitude.

As presented in Fig. 7(a), the ultrasonic power reached the corresponding peak value 42 W at 17.79 kHz. Simultaneously, the ultrasonic amplitude also reached the corresponding maximum value 11.2 μm at 17.79 kHz. Therefore, the idle resonant frequency f_0 of the Ultrasonic 50 was 17.7 kHz and the idle ultrasonic amplitude A_0 was 11.2 μm. Fig. 7(b) demonstrates a positive dependency of ultrasonic power on the ultrasonic amplitude. Through Eq. (23) to fit the data as depicted in Fig. 7(b), the V_{M0} could be derived as 4.25 N/μm.

3.3. Design of RUD tests

The RUD tests were conducted on quartz glass, sapphire crystal and a C/SiC ceramic matrix composite. The dimensions of workpieces for

Table 1
Material properties.

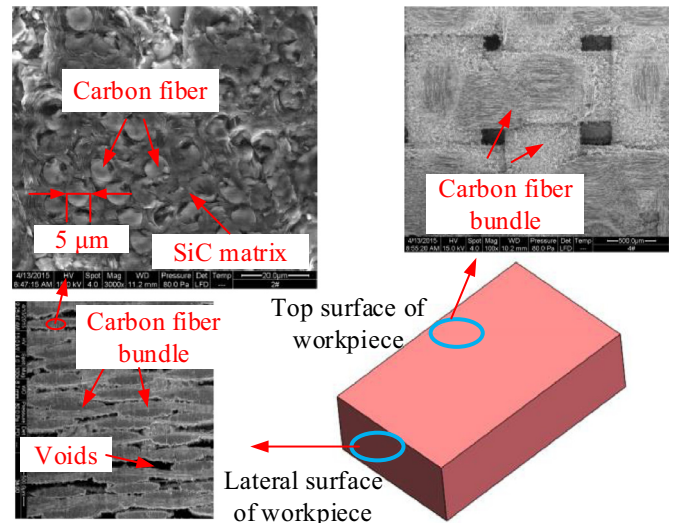| Property	Unit	Quartz glass	Sapphire
Young's modulus	GPa	76.7	478
Vickers hardness	GPa	9.5	27.6
Fracture toughness	MPa m$^{1/2}$	0.71	2.0
Density	g/cm^3	2.2	3.9
Poisson ratio	/	0.17	0.28

Fig. 8. Structure of C/SiC penal.

these three materials were 30 mm × 30 mm × 8 mm. A single hole of 8 mm diameter was drilled in the middle of each workpiece. The quartz glass and sapphire crystal were typical brittle materials of a simple substance. The corresponding mechanical properties are listed in Table. 1. The C/SiC composite was a typical brittle composite material. Fig. 8 presents the structure of the 2D C/SiC panel utilized in this study. It was fabricated by precursor infiltration and pyrolysis. The C/SiC composite consisted of carbon fibers, SiC matrix and voids. The carbon fiber diameter of the C/SiC was approximately 5 μm. Carbon fiber bundles oriented in 0° and 90° could be discriminated from the workpiece surface of approximately 1.8 g/cm^3 in density.

The processing parameters utilized for the RUD tests are listed in Table. 2. The drilling tests were performed twice for each parameter combination. Blaser (Switzerland) supplied the processing coolant uti-

Table 2
Processing variables.

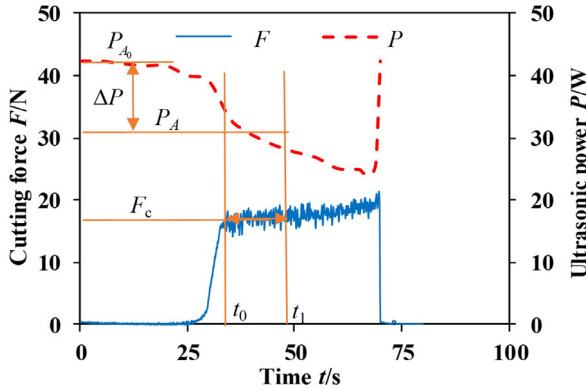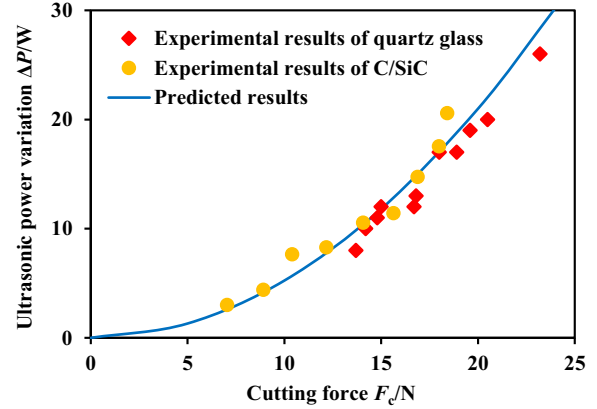| Experiment	Spindle speed (rpm)	Feedrate (mm/min)	Material	Ultrasonic frequency f
Group 3	1000, 3000, 5000	2.4, 3.0, 3.6, 4.2, 5.0, 6.0	Quartz glass	$f \approx f_0 = 17.79$ kHz
Group 4	1000, 3000, 5000	0.5, 1, 1.5	Sapphire	$f \approx f_0 = 17.79$ kHz
Group 5	1000, 3000, 5000	0.3, 0.5, 0.8	C/SiC	$f \approx f_0 = 17.79$ kHz

Fig. 9. Ultrasonic power and cutting force.

Fig. 10. Effect of cutting force on ultrasonic amplitude stability.

Fig. 11. Effect of feedrate on critical cutting force.

lized for the spindle cooling by internal and external circulation in this study.

4. Results

4.1. Verification of cutting force effects on ultrasonic amplitude stability

Fig. 9 presents the typical curves of the time-varying ultrasonic power and cutting force. The average values of the ultrasonic power and cutting force were utilized for the results presentation only in the Section 4.1. These values were calculated by the following system of equations:

$$\begin{cases} P_A = \frac{\int_{t_0}^{t_1} Pdt}{t_1 - t_0} \\ F_c = \frac{\int_{t_0}^{t_1} Fdt}{t_1 - t_0} \end{cases} \tag{28}$$

where, P is the time-varying ultrasonic power, F is the time-varying cutting force, t_0 is the duration when the cutting force first reached a relatively stable value, $t_1 - t_0 = 0.5/f_r$. The factor 0.5 that represented the drilling depth was utilized to ensure a sufficient participation of the abrasives on the material removal. The calculation method of the ultrasonic power variation ΔP is also illustrated in Fig. 9.

Due to positive correlation between the ultrasonic power and the ultrasonic amplitude, the ultrasonic power could be utilized to monitor the ultrasonic amplitude variation. Eq. (24) demonstrates the effects of cutting force on the ultrasonic amplitude stability regardless of material properties when the RUMT was tuned at the corresponding idle resonant frequency. Fig. 10 presents the comparison of predicted results by Eq. (24) with the experimental results on the quartz glass and the C/SiC composite in terms of ultrasonic power variation. As presented in Fig. 10, the predicted results were in good agreement with the experimental results. Simultaneously, despite the quite high difference in material characteristics of the quartz glass and the C/SiC, the experimental results on the quartz glass were consistent with the results on the C/SiC. Therefore, the effect of material properties on the amplitude stability could be attributed to the cutting force variation. The RUD material removal mode should be considered to explain the neglecting difference in the effects of cutting force on the ultrasonic power variation regardless of the material type. Though the quartz glass was a brittle material of simple substance and the C/SiC was a brittle composite, the
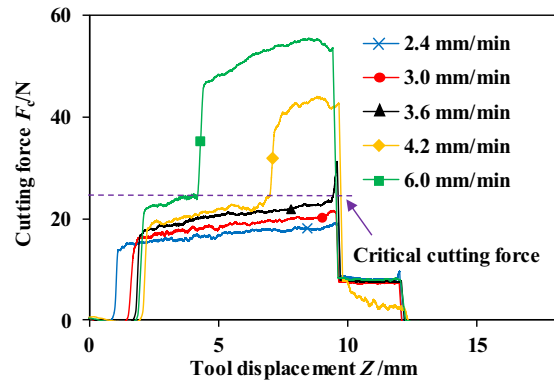
brittle fracture mode was dominant in the quartz glass and C/SiC RUD. Moreover, Eq. (24) was simply derived based on a brittle-fracture-type material removal assumption of the RUD.

4.2. Existence of critical cutting force and repeatability

Fig. 11 presents the cutting force variation during the quartz glass drilling for the spindle speed of 3000 rpm. The most noticeable appearance was the abrupt cutting force increase during drilling when the feedrate was 3.6, 4.2 or 6.0 mm/min. In contrast, when the feedrate was 2.4 or 3.0 mm/min, no such abrupt increase in the cutting force was observed. As it is well known a dramatic reduction of cutting force is the major processing superiority of RUD compared to conventional grinding. The abrupt increase of cutting force suppresses the superiority of RUD. Furthermore, in Fig. 11, the cutting force increased gradually as the drilling depth increased at first for the feedrate of 3.6, 4.2 or 6.0 mm/min. Consequently, when the cutting force exceeds a critical value, the abrupt increase of the cutting force occurs.

Fig. 12 presents the cutting force results of three repeated drilling tests on quartz glass for the feedrate of 6 mm/min and the spindle speed of 3000 rpm. The experimental results demonstrated good repeatability, indicating that the critical cutting force existence was scientifically obligatory rather than accidental.
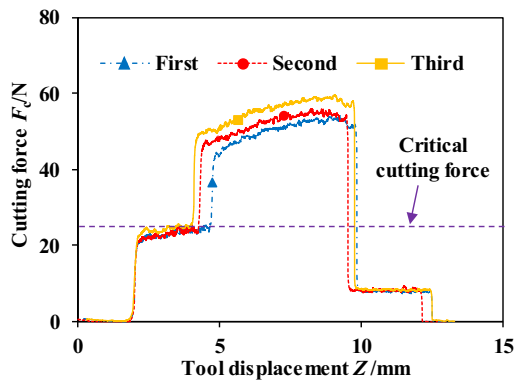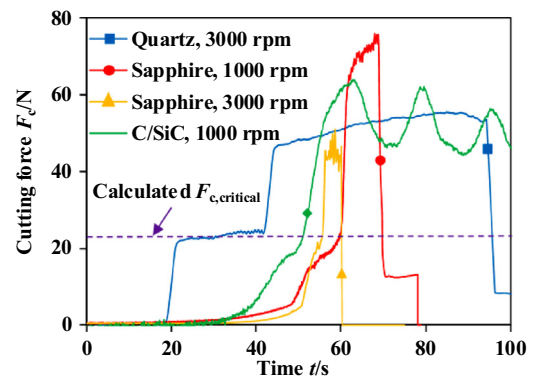
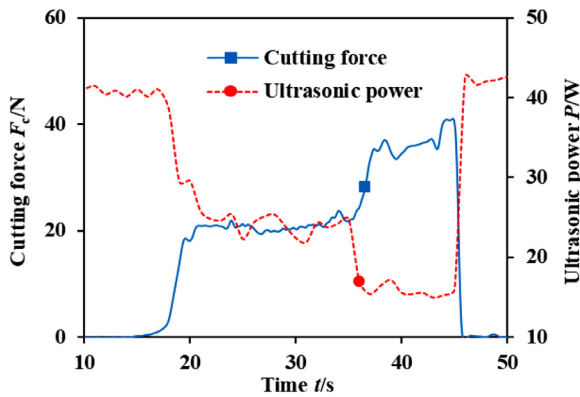**Fig. 12.** Results of repeated experiments.

Fig. 13. Ultrasonic power variation vs cutting force variation.

Fig. 13 presents the ultrasonic power variation during the quartz glass drilling for the feedrate of 5 mm/min and the spindle speed of 5000 rpm. In Fig. 13, the ultrasonic power variation tendency was contrary to the cutting force variation tendency. During drilling, when the cutting force increased abruptly, the ultrasonic power simultaneously decreased abruptly. It indicated that the interaction between the cutting force and the ultrasonic vibration indeed accounted for the critical cutting force existence as demonstrated during the modeling.

4.3. Verification of critical cutting force independency on processing parameters

As demonstrated by Eq. (27), the critical cutting force was only determined by the excitation level $A_0 V_{M0}$ of RUMT. In other words, the critical cutting force ought to be independent of the processing parameters, such as the feedrate, the spindle speed, the material property and even the tool wear.

As presented in Fig. 11, the critical cutting forces for the feedrate of 3.6, 4.2 and 6.0 mm/min were almost identical, indicating that the critical cutting force was independent of the feedrate.

Fig. 14 presents the material and spindle speed effects on the critical cutting force. As illustrated in Fig. 14, indifferently to the materials or to the spindle speed, the critical cutting forces were almost identical. Furthermore, in Fig. 14, the obtained critical cutting force from the experimental results agreed well with the calculated results for V_{M0} of 4.25 N/μm and A_0 of 11.2 μm.

In Fig. 12, the three curves of cutting force did not increase abruptly simultaneously. The occurrence of the cutting force abrupt increase appeared earlier as the drilling sequence increased. Moreover, the cutting force stable value following the abrupt increase increased as the drilling sequence increased. The aforementioned phenomenon indicated a gradual tool wear of RUD. In contrast, the obtained critical cutting forces for

Fig. 14. Effects of material and spindle speed on critical cutting force.

various drilling sequences ere identical, verifying the independency of the critical cutting force on the tool wear.

Therefore, according to the aforementioned discussions, the experimental results verified the theoretical analysis that the 'critical cutting force' was an inherent property of the RUMT and independent of the processing parameters, though the cutting force is truly dependent of processing parameters. In other words, the processing parameters determine the cutting force, but not determine the 'critical cutting force'. The selection of processing parameters should guarantee that the cutting force during the machining process is always smaller than the 'critical cutting force'.

5. Discussion

5.1. Critical cutting force as a novel index for the design and manufacture of RUMT

Because the critical cutting force is an inherent property of RUMT and independent of the processing parameters, it was ideal to be selected as an index for the design and manufacturing of the RUMT. The critical cutting force builds a coupling bridge between the RUD and the RUMT, with consideration to the effect of machining on the ultrasonic vibration stability. It would have two major potential applications:

One was for the design and manufacturing guidance of the RUMT. Ultrasonic frequency and amplitude are two crucial input parameters for process optimization of RUD, therefore two important output indexes for design and manufacturing of RUMT [19,20,37]. Currently, a manufacturer usually only provides these two ultrasonic indexes to users of RUMT. Based on this study, the ultrasonic frequency and amplitude are actually not sufficient to characterize the processing capacity of a RUMT. The manufacturer of RUMT should better provide the corresponding critical cutting force for the users. The potential users can apply the critical cutting force as an index to assist in the selection of RUMT, according to the certain material processing requirement. For harder materials, a RUMT with a higher critical cutting force is required to guarantee the desired machining efficiency. Moreover, given the corresponding good designability of $A_0 V_{M0}$, the manufacturer of RUMT can also design and manufacture the RUMT intentionally and strategically to satisfy any user demands.

The other application of the proposed critical cutting force is for the utilization of a certain RUMT. If only the ultrasonic frequency and amplitude are provided as in the past, the users of a certain RUMT do not know how to select processing parameters guaranteeing the effectiveness of RUD. Due to wrong selection of processing parameters, the RUMT are easily overloaded, resulting in a fatal damage of the RUMT and the workpiece. The transducer of the Ultrasonic 50 utilized in this study was once destroyed when the Si_3N_4 was drilled. In contrast, if the critical cutting force is provided (or obtained by machining experiments), the users of a certain RUMT can not only avoid the aforemen-

tioned problem, whereas can also maximize the RUMT potential by the decisive non-conservative parameters application.

In certain cases, the manufacturer, such as DMG Corp., would provide the ultrasonic power of RUMT to the users. Furthermore, at this time, the users still cannot recognize the RUMT processing capacity simply according to the ultrasonic power. Based on this study, an evaluation method for the critical cutting force calculation could be provided. Through the Eq. (23) substitution into Eq. (27), it could obtain:

$$F_{c,critical} = \frac{P_{A_0} - P_0}{2\pi f_0 A_0 \sqrt{1 + \chi}} \qquad (29)$$

Through Eq. (29), the critical cutting force can be evaluated when the ultrasonic power is provided. Eq. (29) also indicates that only the results of harmonic analysis of the RUMT are not enough to identify its critical cutting force. By the harmonic analysis of the RUMT, the relationship between ultrasonic amplitude A and tuning frequency f can be obtained. Hence the resonant frequency f_0 and maximum ultrasonic amplitude A_0 can be recognized. However, even two RUMTs share same harmonic analysis results with each other, their critical cutting forces are very likely to be different due to their different energy consuming level. Simultaneously, according to Astashev et al. [30], the ultrasonic amplitude A at frequencies in the vicinity of resonance without load can be expressed as: $A = A_0 / \sqrt{1 + (U_M (2\pi f) / V_{M0})^2}$. It can be derived from this equation that, when the A_0, f_0 and A (tuning frequency f) of two RUMTs are all identical correspondingly, the V_{M0} may be distinct due to the difference of U_M. Thus, the information regarding the ultrasonic power is essential to quantificationally identify the critical cutting force of RUMT with the results of harmonic analysis.

According to the critical cutting force modeling and the experimental results, the critical cutting force existence was due to the variation of ultrasonic amplitude during machining. Therefore, for a RUMT that the frequency automatic tracking system was developed, which could retain the output amplitude stable, whereas the existence of critical cutting force ought to be discussed with the frequency automatic tracking system characteristic consideration. In addition, the model of critical cutting force in this study was derived and verified for the RUD of brittle materials. Thus, it could only be convinced that this model was applicable to the RUD process. The applicability of this critical cutting force model to RUFM could not be definitely proposed without experimental data. However, considering their strong similarity of material removal mechanisms between RUD and RUFM, the authors of this study tended to believe the applicability of the critical cutting force model to RUFM. The model verification for RUFM, or whether RUFM has its specific critical phenomenon would be further investigated in the future.

5.2. Methods for RUMT critical cutting force improvement

The critical cutting force model provided a guideline for the critical cutting force improvement of the RUMT. It was enlarging the excitation level $A_0 V_{M0}$ of the RUMT. In order for higher critical cutting force to be obtained, one way was to enlarge A_0 by the input voltage or current increase of the power supply, whereas the other way was to enlarge V_{M0} by of the corresponding ultrasonic vibration system design. Indifferently to the A_0 or V_{M0} enlarging, the ultrasonic power would be enlarged. A higher power RUMT development is beneficial for the RUD of harder materials. In contrast, the enlargement of ultrasonic power follows increased heat production. This indicates that the heat production is inevitable to guarantee the stability of ultrasonic vibration during RUD. In contrast, increased heat production would induce higher temperature variation of the ultrasonic vibration system material. This was harmful for the ultrasonic vibration stability also. In the design of higher power RUMT, it was profitable to pay higher attention to the heat dissipation enhancement than the heat production reduction in order for the temperature variation to be suppressed.

According to Eq. (23), the ultrasonic power is proportional to the square of ultrasonic amplitude A_0, whereas being directly proportional
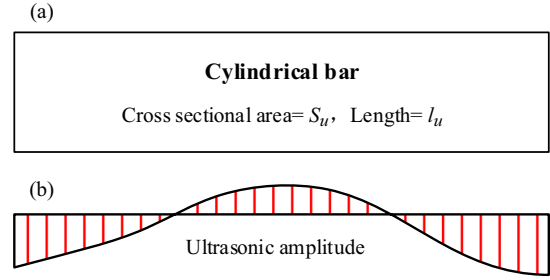
Fig. 15. Model of cylindrical bar vibration system.

to the energy consumption parameter V_{M0} of the RUMT. Thus, the A_0 enlarging is significantly likely to lead an exaggerated temperature variation than the V_{M0} enlargement. Furthermore, the ultrasonic amplitude A_0 is not available to an arbitrary increase with consideration to the dependency of machining performance of the RUD upon it. Therefore, the V_{M0} enlargement is significantly valuable compared to the A_0, when the A_0 is already relatively high.

Following, regarding the designability of V_{M0} a vibration system of a cylindrical bar was taken as an example. Fig. 15 illustrates a model of a cylindrical bar vibration system with the cross sectional area of S_u and the length of l_u.

The $W_M (j\omega)$ of the cylindrical bar vibration system can be expressed as [30]:

$$W_M(j\omega) = \varpi\omega \left(\tan \frac{(\omega_0 - \omega)n\pi}{2\omega_0} + j \frac{\xi_0}{4\pi} \frac{n\pi\omega/\omega_0 - (-1)^n \sin(n\pi\omega/\omega_0)}{1 + (-1)^n \cos(n\pi\omega/\omega_0)} \right) \qquad (30)$$

where, $\omega = 2\pi f$, $\omega_0 = 2\pi f_0$, ϖ is the wave impedance, n is the number of quarter-waves in the length of the bar. ξ_0 is the absorption coefficient of the material that is inversely proportional to the vibrating system Q-factor.

Consequently, the V_{M0} can be derived from Eq. (30) as:

$$V_{M0} = |W_M(j\omega_0)| = \frac{1}{8} \varpi\omega_0 \xi_0 n \qquad (31)$$

With the $\omega_0 = \pi nc/2l_u, c = \sqrt{E_u/\rho_u}$ and $\varpi = S_a\sqrt{E_u\rho_u}$ (c is wave velocity, E_u and ρ_u are elastic module and density of bar material respectively) substitution into Eq. (31), the V_{M0} can be written as:

$$V_{M0} = \frac{S_u E_u \xi_0 \pi n^2}{16 l_u} \qquad (32)$$

Several methods for obtaining higher V_{M0} were demonstrated by Eq. (32), such as the bar cross sectional area enlarging, the number increase of the quarter waves n, and the bar materials with higher absorption coefficient ξ_0 or higher elastic modulus selection. Piezoceramics and giant magnetostrictive materials (GMMs) are the two main types of energy-conversion material in the manufacture of transducers. GMMs have giant magnetostriction (over 1000 ppm), high energy density and higher absorption coefficient than that of piezoceramics. These superior properties of GMMs are beneficial to the miniaturization design of high power RUMT with high critical cutting force. At present, GMMs has been widely applied as energy-conversion materials in the areas such as sonochemistry, industrial processing, and medicine. However, the application of GMMs in the RUMT is very seldom [38]. More efforts are required to prompt the promising utilization of GMMs in RUD technology.

6. Conclusions

In this study, a critical cutting force guaranteeing the superior performance of rotary ultrasonic drilling (RUD) was investigated theoretically and experimentally. The following conclusions could be drawn:

(1) The effect of cutting force on the ultrasonic amplitude stability was modeled when the ultrasonic machine tools (RUMT) were tuned at the corresponding idle resonant frequency. The experimental results on both quartz glass and C/SiC composites verified the model, indicating that the effect of material properties on the amplitude stability could be attributed to the cutting force variation.

(2) During the RUD of brittle materials and composites, when the cutting force exceeded a critical value, it would increase abruptly. Simultaneously, the ultrasonic amplitude would decrease abruptly leading to the severe suppression of the RUD processing superiority in terms of cutting force reduction. A critical cutting force model was developed mechanistically. The experimental results on the quartz glass, the sapphire and the C/SiC composite verified the computational accuracy of the model.

(3) The mechanistic modelling results indicated that the critical cutting force was an inherent property of RUMT depending on the corresponding excitation level, being independent of the processing conditions. The experimental results verified the independency of the critical cutting force of the feedrate, the spindle speed, the material properties and even the tool wear. The critical cutting force is an ideal index for the design and manufacturing of the RUMT, characterizing the corresponding maximum processing capacity.

Acknowledgments

References

[1] Singh RP, Singhal S. Rotary ultrasonic machining: a review. Mater Manuf Process 2016;31:1795–824.

[2] Cong W, Pei Z. Process of ultrasonic machining. In: Nee AYC, editor. Handbook of manufacturing engineering and technology. London: Springer; 2014. p. 1629–50.

[3] Thoe TB, Aspinwall DK, Wise MLH. Review on ultrasonic machining. Int J Mach Tools Manuf 1998;38:239–55.

[4] Zhang C, Cong W, Feng P, Pei Z. Rotary ultrasonic machining of optical k9 glass using compressed air as coolant: a feasibility study. P I Mech Eng B-J Eng 2014;228:504–14.

[5] Wang J, Feng P, Zhang J. Reduction of edge chipping in rotary ultrasonic machining by using step drill: a feasibility study. Int J Adv Manuf Technol 2016;87:2809–19.

[6] Lv D, Zhang Y, Peng Y. High-frequency vibration effects on hole entrance chipping in rotary ultrasonic drilling of bk7 glass. Ultrasonics 2016;72:47–56.

[7] Zhang CL, Feng PF, Pei ZJ, Cong WL. Rotary ultrasonic machining of sapphire: feasibility study and designed experiments. Key Eng Mater 2013;589-590:523–8.

[8] Zeng WM, Li ZC, Pei ZJ, Treadwell C. Experimental observation of tool wear in rotary ultrasonic machining of advanced ceramics. Int J Mach Tools Manuf 2005;45:1468–73.

[9] Feng P, Wang J, Zhang J, Zheng J. Drilling induced tearing defects in rotary ultrasonic machining of c/sic composites. Ceram Int 2017;43:791–9.

[10] Ding K, Fu Y, Su H, Chen Y, Yu X, Ding G. Experimental studies on drilling tool load and machining quality of c/sic composites in rotary ultrasonic machining. J Mater Process Tech 2014;214:2900–7.

[11] Ning FD, Cong WL, Pei ZJ, Treadwell C. Rotary ultrasonic machining of cfrp: a comparison with grinding. Ultrasonics 2016;66:125–32.

[12] Liu J, Zhang D, Qin L, Yan L. Feasibility study of the rotary ultrasonic elliptical machining of carbon fiber reinforced plastics (cfrp). Int J Mach Tools Manuf 2012;53:141–50.

[13] Cong WL, Pei ZJ, Treadwell C. Preliminary study on rotary ultrasonic machining of cfrp/ti stacks. Ultrasonics 2014;54:1594–602.

[14] Qin N, Pei ZJ, Treadwell C, Guo DM. Physics-based predictive cutting force model in ultrasonic-vibration-assisted grinding for titanium drilling. J Manuf Sci Eng 2009;131:41011.

[15] Wang Q, Cong W, Pei ZJ, Gao H, Kang R. Rotary ultrasonic machining of potassium dihydrogen phosphate (kdp) crystal: an experimental investigation on surface roughness. J Manuf Processes 2009;11:66–73.

[16] Singh RP, Singhal S. Rotary ultrasonic machining of macor ceramic: an experimental investigation and microstructure analysis. Mater Manuf Process 2016:1–13.

[17] Zhou M, Wang M, Dong G. Experimental investigation on rotary ultrasonic face grinding of sicp/al composites. Mater Manuf Process 2015;31:673–8.

[18] Xiao X, Zheng K, Liao W. Theoretical model for cutting force in rotary ultrasonic milling of dental zirconia ceramics. Int J Adv Manuf Technol 2014;75:1263–77.

[19] Ferreira PM, Haselkorn M. A mechanistic approach to the prediction of material removal rates in rotary ultrasonic machining. Trans ASME 1995;51:61801.

[20] Liu D, Cong WL, Pei ZJ, Tang Y. A cutting force model for rotary ultrasonic machining of brittle materials. Int J Mach Tools Manuf 2012;52:77–84.

[21] Cong WL, Pei ZJ, Sun X, Zhang CL. Rotary ultrasonic machining of cfrp: a mechanistic predictive model for cutting force. Ultrasonics 2014;54:663–75.

[22] Yuan S, Fan H, Amin M, Zhang C, Guo M. A cutting force prediction dynamic model for side milling of ceramic matrix composites c/sic based on rotary ultrasonic machining. Int J Adv Manuf Technol 2015;86:37–48.

[23] Zhang C, Zhang J, Feng P. Mathematical model for cutting force in rotary ultrasonic face milling of brittle materials. Int J Adv Manuf Technol 2013;69:161–70.

[24] Bertsche E, Ehmann K, Malukhin K. An analytical model of rotary ultrasonic milling. Int J Adv Manuf Tech 2013;65:1705–20.

[25] Wang J, Zhang C, Feng P, Zhang J. A model for prediction of subsurface damage in rotary ultrasonic face milling of optical k9 glass. Int J Adv Manuf Technol 2016;83:347–55.

[26] Wang J, Feng P, Zhang J, Zhang C, Pei Z. Modeling the dependency of edge chipping size on the material properties and cutting force for rotary ultrasonic drilling of brittle materials. Int J Mach Tools Manuf 2016;101:18–27.

[27] Lv D, Huang Y, Tang Y, Wang H. Relationship between subsurface damage and surface roughness of glass bk7 in rotary ultrasonic machining and conventional grinding processes. Int J Adv Manuf Tech 2013;67:613–22.

[28] Geng D, Zhang D, Xu Y, He F, Liu D, Duan Z. Rotary ultrasonic elliptical machining for side milling of cfrp: tool performance and surface integrity. Ultrasonics 2015;59:128–37.

[29] Geng D, Zhang D, Xu Y, He F, Liu F. Comparison of drill wear mechanism between rotary ultrasonic elliptical machining and conventional drilling of cfrp. J Reinf Plast Comp 2014;33:797–809.

[30] Astashev VK, Babitsky VI. Ultrasonic processes and machines. Dynamics, control and applications. Springer Berlin Heidelberg; 2007.

[31] Shamoto E, Moriwaki T. Study on elliptical vibration cutting. Cirp Ann-Manuf Techn 1994;43:35–8.

[32] Wang J, Feng P, Zhang J, Cai W, Shen H. Investigations on the critical feed rate guaranteeing the effectiveness of rotary ultrasonic machining. Ultrasonics 2017;74:81–88.

[33] Jiao F. The theoretical and experimental studies on ultrasonic aided high efficiency lapping with solid abrasive of engineering ceramic Ph. D. thesis. Shanghai Jiao Tong University; 2008.

[34] MARSHALL DB, Abdalla HS. Elastic/plastic indentation damage in ceramics: the lateral crack system. J Am Ceramic Soc-Marshall 1982;65:561–6.

[35] Wang J, Feng P, Zhang J. Experimental investigation on the effects of thermo-mechanical loading on the vibrational stability during rotary ultrasonic machining. Mach Sci Technol 2016.

[36] Nieslony P, Cichosz P, Krolczyk GM, Legutko S, Smyczek D, Kolodziej M. Experimental studies of the cutting force and surface morphology of explosively clad Ti-steel plates. Measurement 2016;78:129–37.

[37] Wang Y, Lin B, Wang S, Cao X. Study on the system matching of ultrasonic vibration assisted grinding for hard and brittle materials processing. Int J Mach Tools Manuf 2014;77:66–73.

[38] Cai W, Zhang J, Yu D, Feng P, Wang J. A vibration amplitude model for the giant magnetostrictive ultrasonic processing system. J Intel Mat Syst Str 2017:1045389X–17711818X.